Original Contribution

Right ventricular myocardial stiffness and relaxation components by kinematic model-based transtricuspid flow analysis in children and adolescents with pulmonary arterial hypertension

Short title: RV stiffness and relaxation in PAH

Yasunobu HAYABUCHI, MD, PhD; Yukako HOMMA, MD; Shoji KAGAMI, MD, PhD

Department of Pediatrics, Tokushima University, Tokushima, Japan

Disclosure

The authors declare that they have no conflicts of interest.

Address for correspondence:

Yasunobu Hayabuchi, MD

Department of Pediatrics, Tokushima University

Kuramoto-cho-3, Tokushima 770-8305, Japan

Tel: +81-886-33-7135; Fax: +81-886-31-8697

E-mail: hayabuchi@tokushima-u.ac.jp

Abstract

We hypothesized that the kinematic model-based parameters obtained from the transtricuspid E-wave would be useful for evaluating RV diastolic property in pediatric pulmonary arterial hypertension (PAH) patients. The model was parametrized by stiffness/elastic recoil k, relaxation/damping c, and load x. These parameters were determined as the solution of $m \cdot d^2x/dt^2 + c \cdot dx/dt + kx = 0$, which is based on the theory that the E-wave contour is determined by the interplay of stiffness/restoring force, damping/relaxation force, and load. The PAH group had a significantly higher k and c versus the control group (182.5 ± 72.4 g/s2 vs. 135.7 ± 49.5 g/s2, p = 0.0232 and 21.9 ± 6.5 g/s vs. 10.6 ± 5.2 g/s, p <0.0001, respectively). These results show that RV has a higher stiffness/elastic recoil and inferior cross-bridge relaxation in the PAH group. Present findings indicate the feasibility and utility of kinematic model parameters for assessing RV diastolic function.

Key words:

Right ventricle; diastolic function; pulmonary arterial hypertension

Introduction

Systemic hypertension is recognized as one of the major causes of diastolic dysfunction in the left ventricle (LV) (Marwick et al. 2015). However, there is limited knowledge regarding the effect of chronic pressure overload on the right ventricular (RV) diastolic function. Since the assessment of the RV diastolic function is challenging (Rain et al. 2016: Murch et al. 2015), only a few studies have investigated the RV diastolic function, particularly in pediatric pulmonary arterial hypertension (PAH) patients (Okumura et al. 2014). Thus, development of an accurate measurement of the RV diastolic dysfunction might help contribute to an improved clinical management of these patients (Shiina et al. 2009; Yang W et al. 2018).

Noninvasive assessment of diastolic function is commonly achieved through the use of pulsed Doppler echocardiography. Although conventional echocardiographic parameters are often indicative of dysfunction, their utility in characterizing the relaxation and stiffness/elastic recoil is limited (Cosson and Kevorkian JP 2003). To overcome the limitations of these parameters, Kovács et al. quantified LV diastolic function using a mechanistic model of filling that was determined by cross-bridge uncoupling relaxation, elastic recoil/restoring forces, and initial displacement (load) (Kovács et al. 1987; Bauman et al. 2004; Shmuylovich and Kovács 2006). Based on these findings, we attempted to further evaluate the RV diastolic function by analyzing the transtricuspid E-waves using the parametrized diastolic filling (PDF) formalism. We recently demonstrated the feasibility and usefulness of kinematic model parameters obtained from RV pressure waveform for evaluating RV diastolic function (Hayabuchi et al. 2018). It showed that the PAH group had higher stiffness/restoring and inferior cross-bridge relaxation than the control group. However, these results in our previous studies are obtained by invasive examination. In this investigation, noninvasive assessment by using pulsed Doppler E-wave was examined in PAH patients.

We hypothesized that the physical and physiological principles govern the transtricuspid flow pattern and that a mathematical model would be able to correctly quantify the pathological RV diastolic property in children and adolescents with PAH.

Materials and Methods

Study Population

This prospective study enrolled 10 consecutive pediatric idiopathic PAH patients (PAH group; mean age ± standard deviation [SD], 12.8 ± 5.4 years; age range, 8-19 years). We also enrolled 34 consecutive age-matched healthy subjects without chest X-rays and electrocardiographic or echocardiographic abnormalities (control group; mean age, 11.3 ± 3.4 years; age range, 7-19 years).

Data analyzed in the study were collected from December 2013 to October 2017. All study protocols conformed to the ethical guidelines of the Declaration of Helsinki (1975) and were approved by the Institutional Review Board of Tokushima University Hospital. Written, informed consent for their children to participate in the study was provided by the parents.

Echocardiography

Standard and pulsed Doppler echocardiography was performed using a Preirus digital ultrasound system (Hitachi-Aloka Medical Co., Tokyo, Japan) equipped with 1–5- and 3–7-MHz sector transducers. All Doppler data were acquired from patients in the left lateral decubitus position during shallow respiration or end-expiratory apnea. Participants were assessed by conventional, M-mode, pulsed, and color Doppler echocardiography. Transmitral and transtricuspid diastolic blood flow velocities were determined in the apical 4-chamber view by placing the pulsed Doppler sample volume at the tip of the valve leaflets. Mitral and tricuspid annular velocities were recorded

using the pulsed wave tissue Doppler imaging (TDI) technique. The conventional echocardiographic parameters that were measured included: E-wave acceleration time (AT), deceleration time (DT), peak E- and A-wave velocities (E-peak and A-peak, respectively), and the E/A ratio. Peak early mitral and tricuspid annular velocity (e′) and peak late annular velocity (a′), E/e′, and e′/a′ were similarly calculated from the Doppler tissue recordings. Values were calculated for each of the 5 wave images in each subject and then averaged.

Doppler E-wave analysis using kinematic model

For each subject, 5 transmitral and transtricuspid E- and A-waves were selected. Transmitral and transtricuspid E-waves were evaluated as follows. Using a custom MATLAB release 2015a (MathWorks, Natick, MA, USA) program, beats with clear contours were selected, digitized, and cropped. The maximum velocity envelope was determined from the digitized E-wave image and then used to obtain the automated PDF fit. For the purpose of detecting the appropriate velocity profile, the program searches each time point of the image from the top down for the first pixel having a brightness higher than or equal to a user defined threshold level, matching each time point with a velocity. Furthermore, it is assumed that there must be an upper limit to the velocity difference between two time points a few milliseconds apart. The algorithm accordingly discards a detected velocity that differs too much from the previous velocity. Discarded velocities are displayed for reference and transparency as to the behavior of the algorithm.

The E-waves were then used to compute the PDF parameters. The PDF formalism characterizes the suction-initiated transmitral or transtricuspid flow. This is analogous to the kinematics of a previously displaced, damped, harmonic oscillator after it recoils from a resting state. This methodology utilizes Newton's Second Law, with the

predictions of the E-wave contours parametrized on the basis of the chamber stiffness, relaxation/viscoelasticity, and the load. The equation that describes the balance of forces in a damped harmonic oscillator is:

$$m\frac{\mathrm{d}^2x}{\mathrm{d}t^2} + c\frac{\mathrm{d}x}{\mathrm{d}t} + kx = 0 \qquad (1)$$

where m (g), c (g/s) and k (g/s^2) represent inertia, relaxation (damping) and ventricular stiffness/elastic recoil (spring constant), respectively. The parameter x_0 (cm) indicates the load and represents the initial displacement of the spring before motion, which corresponds to the elastic strain stored in the myocardium and surrounding structures available at the mitral or tricuspid valve openings that facilitate the mechanical recoil (Kovács et al. 1987; Bauman et al. 2004; Shmuylovich and Kovács 2006). When the initial velocity (dx/dt) of the system is zero, this corresponds to no transmitral or transtricuspid flow prior to the valve opening. The inertial term m (g) is normalized to 1 in order to enable the computation of c and k per unit mass. These parameters (k, c, and x_0) can be directly determined from the clinical E-wave contour. The estimated model parameters are averaged values within the cardiac phase of interest. Expressions describing the velocity of motion as a function of time are derived from the foundational equation (1). For underdamped cases, which are defined by $c^2 - 4k < 0$, the expression for the velocity (v) as a function of time (t) is

$$v(t) = \frac{-kx_0}{\omega}\, exp(-c\cdot t/2)\cdot\sin(\omega\cdot t) \quad , \qquad (2)$$

where

$$\omega = \sqrt{4k - c^2}/2 .$$

For the overdamped cases, which are defined by $c^2 - 4k > 0$, the expression is

$$v(t) = \frac{-kx_0}{\beta} exp(-c \cdot t/2) \cdot \sin(\beta \cdot t) \quad , \qquad (3)$$

where

$$\beta = \sqrt{c^2 - 4k}/2 .$$

For critically damped cases, which are defined by $c2 - 4k = 0$, the expression is

$$v(t) = -kx_0 \cdot t \cdot exp(-c \cdot t/2) . \qquad (4)$$

The output of the Levenberg–Marquardt algorithm is used to determine the PDF parameter values for k, c, and x_0, while the E-wave maximum velocity envelope is used as the input via a custom LabVIEW 2016 (National Instruments, Austin, TX, USA) interface. The gold-standard methods (simultaneous micromanometric hemodynamics and echocardiography) have been extensively used to validate the physiological interpretation. Results have shown these parameters are causally related to the chamber properties that determine diastolic function (Kovács et al. 1987; Kovács et al. 1997; Kovács et al. 2000; Lisauskas et al. 2001). Physiological conditions can additionally be determined from the damped harmonic oscillator derived parameters such as kx_0, which is the peak force in the spring that corresponds to the peak atrioventricular pressure gradient that generates the E-wave (Kovács et al. 1987; Bauman et al. 2004) ; $1/2kx_0^2$, which indicates the stored potential elastic energy that is capable of generating the recoil (Kovács et al. 1987); the peak resistive force (cE-peak),

which is the force that resists filling at the peak flow; and c^2-4k, which indicates the balance between the factors both driving and resisting the ventricular filling (Kovács et al. 1987; Bauman et al. 2004; Shmuylovich and Kovács 2006). The consecutive 5 selected beats in each subject were used to calculate the c, k, and x_0 averages, as well as the other indexes that corresponded to the determinants of the E-wave.

In the first step of our study, we compared the kinematic model parameters c, k, and x_0 between the LV and the RV in the control group in order to assess the characteristics of the normal RV diastolic physiology. Subsequently, results from the E-waves in the PAH group were compared with those obtained from the normal RV to elucidate the RV diastolic pathophysiology during the RV pressure overload.

Statistical analysis

All data are expressed as mean ± SD or as median with range from the minimum to maximum. The significance of difference was determined using the Mann-Whitney *U*-test or Student's *t*-test, as appropriate. Linear regression analyses were performed for correlations between the kinematic parameters and hemodynamic parameters, and Pearson's correlation coefficients were calculated. All statistical data were analyzed using Prism (version 6.0; GraphPad Software, San Diego, CA, USA) and JMP 11 (SAS Institute, Inc., Cary, NC, USA). $P < 0.05$ (2-sided) was considered to indicate significance. Intra-observer variability was assessed by one investigator, who conducted measurements on the same patients 8 weeks apart, while the inter-observer variability was assessed by a second investigator who was unaware of the previous results and performed the same measurements on 20 randomly selected participants. Intra- and inter-observer agreements were assessed using intraclass correlation coefficients (ICCs). In addition, agreement between investigators was tested using a

Bland-Altman analysis by calculating the bias (mean difference) and 1.96 SD around the mean difference.

Results

None of the subjects were excluded from the analysis due to suboptimal Doppler E-wave recordings. As a result, the study population comprised 10 PAH patients (PAH group; mean age ± SD, 12.8 ± 5.4 years; age range, 8–19 years) and 34 healthy subjects (control group; 11.3 ± 3.4 years; 7–19 years). Table 1 presents the participants' clinical and echocardiographic data, along with the ranges. The groups were well matched, and no statistically significant differences were observed between the groups for any of the clinical categories. Figure 1 shows 2 representative examples of transtricuspid Doppler E-wave velocity profile edge detection and fitted curves. These examples demonstrate the method and process on how the digitized E-wave image was used to determine the maximum velocity envelope, from which the automated PDF fit was obtained.

PDF indexes of normal LV and RV in the control group

The kinematic model parameters were compared between the normal LV and RV. In the control group, k, c, and x_0 were significantly lower in the normal RV versus the normal LV (Table 2). These results indicate that normal RV exhibits lower stiffness/elastic recoil, superior cross-bridge relaxation, and a lower initial load. Model validation was assessed in all 34 participants. During the assessment of the kinematic model fit, there was a consistent and significantly lower mean square error (MSE, cm^2/s^2) for the RV versus the LV, thereby demonstrating that a mathematical difference between the detected envelop and the fitting curve is smaller. This might result from the fine fitting of RV diastolic performance to the PDF model, or less noise/scattering in

the ultrasound signal of the transtricuspid flow.

Conventional RV diastolic parameters in the control and PAH groups

Table 3 shows the conventional and kinematic model-based diastolic parameters in the control and PAH groups. The E-peak was significantly lower, whereas the A-peak was significantly higher in the PAH versus the control group. Similarly, the value of e′ was significantly lower, while a′ was significantly higher in the PAH group. E-waves of the PAH group revealed there was a significantly shorter AT, whereas there was no significant difference found between the PAH and control subjects for DT. Furthermore, there was no significant difference for the value of E/e′ between the 2 groups. Guidelines for the echocardiographic assessment of the right heart from the American Society of Echocardiography (ASE) recommend using the 3 Doppler parameters, E/A, E/e′, and DT, for the evaluation of RV diastolic dysfunction (Rudski et al. 2010). The normal range of E/A has been shown to be 0.8 to 2.1, with an E/e′ >6 and DT <120 ms defined as indicative of an abnormal diastolic function. Since these criteria are adapted for adults, we understand that assessments using these criteria could be relatively problematic in our subjects (Rudski et al. 2010; Berman et al. 1990; Innelli et al. 2009: Zoghbi et al. 1990). Our results showed that only the E/A ratio exhibited a significant difference between the control and PAH groups, whereas there was no significant difference in E/e' and DT (Fig.2A-C).

Kinematic model-based diastolic parameters of the RV in the PAH group

As compared to the control group, the PAH group exhibited significantly greater values for the parameters k (182.5 ± 72.4 g/s^2 vs. 135.7 ± 49.5 g/s^2, $p = 0.0232$) and c (21.9 ± 6.5 g/s vs. 10.6 ± 5.2 g/s, $p < 0.0001$). These results demonstrate that the PAH RV has a higher stiffness and inferior active relaxation in diastole. The PAH and

control groups had an indistinguishable initial load prior to the tricuspid valve opening (x_0: 7.7 ± 2.4 cm in PAH; 8.2 ± 2.9 cm in the control group) (Fig. 2D-F). The PAH group also exhibited greater values of cE-peak, kx_0, and $1/2kx_0^2$ (Table 3).

Correlation between kinematic parameters and RV performance in the PAH group

In order to analyze the relationships between the kinematic –based parameter values and PAH severity and RV systolic performance, we evaluated the correlation between kinematic parameters and RVFAC (right ventricular fractional area change) and TRPG (tricuspid regurgitation peak gradient) (Fig. 3A-F). RVFAC did not have significant correlation with k, c, and x_0. Although there was significant correlation between TRPG and k ($r = 0.778$, $p = 0.0008$), TRPG did not have significant correlation with c and x_0.

Reproducibility

To assess the reproducibilities of the conventional and the kinematic parameters, intra- and inter-observer variabilities in the measurements were confirmed in 20 randomly selected participants (15 control and 5 PAH) by means of ICCs and Bland-Altman analysis (Table 4). With the exception for the AT, the ICCs of the kinematic model-based parameters, k, c, and x_0, for intra- and inter-observer variabilities were relatively lower than conventional parameters, which included the E-peak, A-peak, DT, e′, and a′. However, the Bland-Altman analysis showed there was a minimal bias physiologically and clinically, in addition to a substantial agreement for reproducibility.

Discussion

The present study demonstrated that the causality-based RV diastolic function

assessment by analysis of the transtricuspid E-waves via the PDF method generated parameters of chamber stiffness/elastic recoil and relaxation/viscosity that could be differentiated between the PAH patients and the age-matched control subjects.

The parameter k represents the chamber stiffness/elastic recoil property. Due to its thin wall, the RV is considered to be a passive compliant chamber, and thus, the parameter k of the RV was found to be much lower than that for the LV in the control group. Recent studies have demonstrated RV hypertrophy with extracellular collagen deposition (Rain et al. 2013), increased sarcomeric stiffness ((Rain et al. 2014), and changes in the giant elastic protein titin isoform and phosphorylation (LeWinter and Granzier 2010; Anderson et al. 2010; Hidalgo et al. 2009; Hudson et al. 2010), which contributes closely to stiffening of the cardiomyocytes.

Chamber stiffness (dP/dV) as evaluated by invasive cardiac catheterization, has been shown to be linearly related to the spring constant k (g/s^2) (Kovács et al. 1997; Kovács et al. 2001; Lisauskas et al. 2001). It has been shown that PDF analysis of the Doppler E-wave can accurately determine the LV diastatic passive chamber stiffness (Mossahebi and Kovács 2012). The higher k value for the RV in the PAH group is consistent with an elevated RV filling pressure.

Kinematically, the lumped viscoelastic (resistive) properties of the system are represented by the c parameter. Thus, any source of energy loss that opposes motion during the filling are considered to be a part of the physiological analog. Increased values of c can be manifested by various factors that can influence filling via an energy loss. These factors can include blood viscosity, delayed relaxation, dynamic friction during sarcomere lengthening that occurs as the detached myosin heads slide past the thin filaments, pericardial effects, and the viscosity of the extracellular matrix (Dent et al. 2001; Kass 2003; Chung et al. 2011). Changes in intracellular calcium handling and high myofilament calcium sensitivity in PAH have been reported to impair proper

relaxation of cardiomyocytes (Rain et al. 2016). Moreover, these pathological conditions are known to affect the kinematic model parameters.

The x_0 value is related to the load responsible for compressing the elastic myocardium at the end of systole, which is a prerequisite in order for the restoring force to arise. The x_0 value is also closely related to the velocity time integral (VTI) of the E-wave. In normal subjects, the parameter x_0 was lower in the RV versus the LV. This might be because of the difference of the area at the tip of the valve leaflets found between them. Furthermore, this could possibly be due to the difference of the E/A ratio, Doppler beam angle, and respiratory condition present at the time of the recording. In our current study, there was no significant difference in the volumetric preload parameter x_0 between the control and PAH groups. This value is specifically determined by several factors, including stroke volume, volumetric E/A ratio, RV filling pressure, and right atrial pressure. This finding suggests that during pathological conditions, these PAH patients maintained the stroke volume while at rest.

To the best of our knowledge, this is the first application of kinematic model parameters obtained from transtricuspid E-wave contours for use in assessing RV diastolic function. Our data also showed that the initial maximum recoil force (kx_0) and the stored potential elastic energy ($1/2kx_0^2$) were significantly higher in the PAH versus the control group. The product kx_0, which is analogous to the maximum atrioventricular pressure gradient that generates the E-wave by mechanical suction, represents the initial peak force in the spring. The results of a previous investigation that found the kx_0 was more consistent than the modified Bernoulli equation ($PG = 4V^2$; PG, pressure gradient; V, blood flow velocity) with regard to predicting the instantaneous maximum pressure gradient also validates the above predictions (Bauman et al. 2004).

Kinematically, the potential energy in the spring prior to its release is represented by $1/2kx_0^2$. The physiological analog for this factor is the stored elastic

strain energy that is available at the tricuspid valve opening. This energy generates the chamber recoil, which leads to the generation of the E-wave. The significantly greater values for kx_0 and $1/2kx_0^2$ in the PAH group suggest that an adaptive mechanism via the hypertrophic RV chamber is required in order to maintain a stroke volume. This is shown by our results that indicated that there was no significant difference for the load x_0 between the control and PAH groups. However, this occurs at the cost of increased energy utilization. In addition, our data also indicated that the cE-peak was significantly higher in the PAH patients versus the control subjects, which indicates a higher resistance (impaired relaxation) to the RV filling. A greater atrioventricular pressure gradient kx_0 (and consequently, $1/2kx_0^2$) would be expected to be generated in response to increased damping (resistive losses) of the transtricuspid flow, as is manifested by greater values of c and cE-peak, in order to maintain the load x_0 or stroke volume.

Although previous reports and the ASE guidelines have suggested the usefulness of conventional parameters in the assessment of RV diastolic dysfunction (Okumura et al. 2014; Rudski et al. 2010; Sade et al. 2007; Sundereswaran et al. 1998; Leeuwenburgh et al. 2002), the utilization of these parameters has remained controversial (Sade et al. 2007; Sundereswaran et al. 1998; Leeuwenburgh et al. 2002). The present study revealed that E/e′ and DT of the transtricuspid E-wave did not exhibit any significant differences between the control and PAH groups, whereas there was a significant difference for the E/A. This discrepancy regarding the usefulness of the conventional indexes might be associated with the subjects' age, disease duration, and pathological severity. Moreover, the progression of the RV diastolic function deterioration, which consists of active relaxation and stiffness/elastic recoil, might differ between children and adults.

In most of the studies that have examined these differences, results indicated

there was a modest correlation between the E/A ratio and increasing age (Innelli et al. 2009; Zoghbi et al. 1990). Since the peak velocity of E-wave increases during inspiration, this causes an increase in the E/A ratio. Furthermore, while increases in the E-peak are caused by tachycardia, a relatively greater increase in the A-peak will result in a decrease in the E/A ratio (Zoghbi et al. 1990; Yu et al. 2003).

These parameters are also sensitive to changes in preload. Thus, while a reduction in the preload will lead to a decrease in E, there will be a relatively smaller decrease in A, thereby causing the E/A to decrease (Guazzi et al. 2000; O'Sullivan et al. 2005; Pelà et al. 2004). However, it should be noted that since the conventional echocardiographic diastolic function indexes are empirical, these values will not provide any mechanistic information on the chamber property, e.g., stiffness and relaxation. Moreover, since E-wave parameters are not derived from basic physiologic principles that govern filling, these parameters are considered to be load dependent (King et al. 2008; Paelinck et al. 2003; Pepi et al. 2000). In addition, the complex interplay of simultaneous physiologic determinants and chamber properties are responsible for generating these indexes (such as E/A). Moreover, a previous study has demonstrated that E-wave DT was specifically dependent upon both the chamber stiffness and the chamber relaxation/viscoelasticity (Shmuylovich and Kovács 2007).

We applied the PDF formalism in order to elucidate the RV diastolic property in the present investigation. In this study, we attempted to characterize the kinematic properties of the diastolic chamber. In order to define the individual components of each E-wave, we used the digitized E-wave contour as input, along with the best-fit, mathematically unique (c, k, and x_0) parameters. All the global physiologic determinants of the contour were accounted for by the 3 lumped parameters c, k, and x_0. RV diastolic dysfunction determines ventricular performance and patient outcomes for many conditions. Moreover, this dysfunction may precede the apparent systolic

dysfunction (Rudski et al. 2010; Leeuwenburgh et al. 2002; Dernellis 2001; Gan et al. 2007).

Overall, we believe that our current findings indicate that there are great clinical implications for this method with regard to the management of PAH patients.

Study limitations

As the aim of the present study was to establish the kinematic parameters as RV diastolic functional indexes, we attempted to validate these parameters by evaluating the normal LV, normal RV, and PAH RV diastolic function. Although we analyze the relation between the parameter values and the PAH severity (TRPG), only the parameter k was correlated with TRPG. RVFAC did not have significant correlation with k, c, and x_0. We consider that since the present study population was small, and the patients' clinical courses and treatment were heterogeneous, it might be not appropriate to undertake a detailed analysis with sufficient statistical power to detect statistically reliable signifincance. Further studies will be needed in order to determine whether these parameters might be useful evaluation tools and could become the gold standard for assessing RV diastolic function and for predicting the prognosis of patients with this disease.

In the present investigation, we did not perform invasive cardiac catheterization examination to confirm the feasibility of the kinematic model indexes. However, with the combined pressure conductance catheter, it has become possible to simultaneously determine the ventricular pressure and volume. Since this gold standard method for measuring load-independent diastolic stiffness by pressure-volume (PV) analysis requires temporal preload reduction, this procedure is not without risk in PAH patients (Senzaki and Kass 2010). However, the development of single-beat analyses of the diastolic PV relationship have helped to circumvent this issue in left

heart failure patients (Klotz et al. 2006). Even so, whether the use of this analysis can be conducted for the RV in PAH patients remains unclear. Furthermore, it can be quite difficult to assess the RV diastolic function when using PV analysis, as precise RV volumetric measurements are also challenging. Moreover, unlike for stiffness (dP/dV), currently there is no simple catheterization-based analog that can be used for the relaxation parameter c. As a result, it might not necessarily be useful to perform cardiac catheterization in order to confirm the utility of these model-based parameters.

Conclusions

This study demonstrated the feasibility and usefulness of the causality-based kinematic model parameters obtained from the transtricuspid E-wave contours for characterizing the RV diastolic pathophysiological property.

Disclosures

None.

References

Anderson BR, Bogomolovas J, Labeit S, Granzier H. The effects of PKCalpha phosphorylation on the extensibility of titin's PEVK element. *J Struct Biol* 2010;170:270–277.

Bauman L, Chung CS, Karamanoglu M, Kovács SJ. The peak atrioventricular pressure gradient to transmitral flow relation: kinematic model prediction with in vivo validation. *J Am Soc Echocardiogr* 2004;17:839–844.

Berman GO, Reichek N, Brownson D, Douglas PS. Effects of sample volume location, imaging view, heart rate and age on tricuspid velocimetry in normal subjects. *Am J Cardiol* 1990;65:1026–1030.

Chung CS, Methawasin M, Nelson OL, Radke MH, Hidalgo CG, Gotthardt M, Granzier HL. Titin based viscosity in ventricular physiology: an integrative investigation of PEVK-actin interactions. *J Mol Cell Cardiol* 2011;51:428-434.

Cosson S, Kevorkian JP. Left ventricular diastolic dysfunction: an early sign of diabetic cardiomyopathy? *Diabetes Metab* 2003;29:455–466.

Dent CL, Bowman AW, Scott MJ, Allen JS, Lisauskas JB, Janif M, Wickline SA, Kovács SJ. Echocardiographic characterization of fundamental mechanisms of abnormal diastolic filling in diabetic rats with a parameterized diastolic filling formalism. *J Am Soc Echocardiogr* 2001;14:1166–1172.

Dernellis J. Right atrial function in hypertensive patients: effects of antihypertensive therapy. *J Hum Hypertens* 2001;15:463–470.

Gan CT, Holverda S, Marcus JT, Paulus WJ, Marques KM, Bronzwaer JG, Twisk JW, Boonstra A, Postmus PE, Vonk-Noordegraaf A. Right ventricular diastolic dysfunction and the acute effects of sildenafil in pulmonary hypertension patients. *Chest* 2007;132:11–17.

Guazzi M, Maltagliati A, Tamborini G, Celeste F, Pepi M, Muratori M, Berti M, Guazzi MD. How the left and right sides of the heart, as well as pulmonary venous drainage, adapt to an increasing degree of head-up tilting in hypertrophic cardiomyopathy: differences from the normal heart. *J Am Coll Cardiol* 2000;36:185–193.

Hayabuchi Y, Ono A, Homma Y, Kagami S. Analysis of Right Ventricular Myocardial Stiffness and Relaxation Components in Children and Adolescents With Pulmonary Arterial Hypertension. J Am Heart Assoc. 2018 Apr 19;7(9). pii: e008670.

Hidalgo C, Hudson B, Bogomolovas J, Zhu Y, Anderson B, Greaser M, Labeit S, Granzier H. PKC phosphorylation of titin's PEVK element: a novel and conserved pathway for modulating myocardial stiffness. *Circ Res* 2009;105:631–638.

Hudson BD, Hidalgo CG, Gotthardt M, Granzier HL. Excision of titin's cardiac PEVK spring element abolishes PKCalpha-induced increases in myocardial stiffness. *J Mol Cell Cardiol* 2010;48:972–978.

Innelli P, Esposito R, Olibet M, Nistri S, Galderisi M. The impact of ageing on right ventricular longitudinal function in healthy subjects: a pulsed tissue Doppler study. *Eur J Echocardiogr* 2009;10:491–8.

Kass DA. Getting better without AGE: New insights into the diabetic heart. *Circ Res* 2003;92:704 –706.

King GJ, Murphy RT, Almuntaser I, Bennett K, Ho E, Brown AS. Alterations in myocardial stiffness in elite athletes assessed by a new Doppler index. *Heart* 2008;94:1323–1325.

Klotz S, Hay I, Dickstein ML, Yi GH, Wang J, Maurer MS, Kass DA, Burkhoff D. Single-beat estimation of end-diastolic pressure-volume relationship: a novel method with potential for noninvasive application. *Am J Physiol Heart Circ Physiol* 2006;291:H403–412.

Kovács SJ Jr., Barzilai B, Perez JE. Evaluation of diastolic function with Doppler

1 echocardiography: the PDF formalism. *Am J Physiol* 1987;252:H178–187.
2 Kovács SJ, Meisner JS, Yellin EL. Modeling of diastole. *Cardiol Clin* 2000;18:459–487.
3 Kovács SJ, Setser R, Hall AF. Left ventricular chamber stiffness from model-based
4 image processing of transmitral Doppler E-waves. *Coron Artery Dis* 1997;8:179–187.
5 Leeuwenburgh BP, Steendijk P, Helbing WA, Baan J. Indexes of diastolic RV function:
6 load dependence and changes after chronic RV pressure overload in lambs. *Am J*
7 *Physiol Heart Circ Physiol* 2002;282:H1350–1358.
8 LeWinter MM, Granzier H. Cardiac titin: a multifunctional giant. *Circulation*
9 2010;121:2137–2145.
10 Lisauskas JB, Singh J, Bowman AW, Kovács SJ. Chamber properties from transmitral
11 flow: prediction of average and passive left ventricular diastolic stiffness. *J Appl*
12 *Physiol (1985)* 2001;91:154–162.
13 Marwick TH, Gillebert TC, Aurigemma G, Chirinos J, Derumeaux G, Galderisi M,
14 Gottdiener J, Haluska B, Ofili E, Segers P, Senior R, Tapp RJ, Zamorano JL..
15 Recommendations on the use of echocardiography in adult hypertension: A report
16 from the European Association of Cardiovascular Imaging (EACVI) and the
17 American Society of Echocardiography (ASE). *Eur Heart J Cardiovasc Imaging*
18 2015;16:577-605.
19 Mossahebi S, Kovács SJ. Kinematic modeling-based left ventricular diastatic (passive)
20 chamber stiffness determination with in-vivo validation. *Ann Biomed Eng*
21 2012;40:987–995.
22 Murch SD, La Gerche A, Roberts TJ, Prior DL, MacIsaac AI, Burns AT. Abnormal right
23 ventricular relaxation in pulmonary hypertension. *Pulm Circ* 2015;5:370–375.
24 Okumura K, Slorach C, Mroczek D, Dragulescu A, Mertens L, Redington AN, Friedberg
25 MK. Right ventricular diastolic performance in children with pulmonary arterial
26 hypertension associated with congenital heart disease: correlation of

echocardiographic parameters with invasive reference standards by high-fidelity micromanometer catheter. *Circ Cardiovasc Imaging* 2014;7:491–501.

O'Sullivan CA, Duncan A, Daly C, Li W, Oldershaw P, Henein MY. Dobutamine stress-induced ischemic right ventricular dysfunction and its relation to cardiac output in patients with three-vessel coronary artery disease with angina-like symptoms. *Am J Cardiol* 2005;96:622–627.

Paelinck BP, van Eck JW, De Hert SG, Gillebert TC. Effects of postural changes on cardiac function in healthy subjects. *Eur J Echocardiogr* 2003;4:196–201.

Pelà G, Regolisti G, Coghi P, Cabassi A, Basile A, Cavatorta A, Manca C, Borghetti A. Effects of the reduction of preload on left and right ventricular myocardial velocities analyzed by Doppler tissue echocardiography in healthy subjects. *Eur J Echocardiogr* 2004;5:262–271.

Pepi M, Guazzi M, Maltagliati A, Berna G, Tamborini G. Diastolic ventricular interaction in normal and dilated heart during head-up tilting. *Clin Cardiol* 2000;23:665–672.

Rain S, Andersen S, Najafi A, Gammelgaard Schultz J, da Silva Gonçalves Bós D, Handoko ML, Bogaard HJ, Vonk-Noordegraaf A, Andersen A, van der Velden J, Ottenheijm CA, de Man FS. Right ventricular myocardial stiffness in experimental pulmonary arterial hypertension: relative contribution of fibrosis and myofibril stiffness. *Circ Heart Fail* 2016;9:e002636.

Rain S, Bos Dda S, Handoko ML, Westerhof N, Stienen G, Ottenheijm C, Goebel M, Dorfmüller P, Guignabert C, Humbert M, Bogaard HJ, Remedios CD, Saripalli C, Hidalgo CG, Granzier HL, Vonk-Noordegraaf A, van der Velden J, de Man FS. Protein changes contributing to right ventricular cardiomyocyte diastolic dysfunction in pulmonary arterial hypertension. *J Am Heart Assoc* 2014;3:e000716.

Rain S, Handoko ML, Trip P, Gan CT, Westerhof N, Stienen GJ, Paulus WJ, Ottenheijm

CA, Marcus JT, Dorfmüller P, Guignabert C, Humbert M, Macdonald P, Dos Remedios C, Postmus PE, Saripalli C, Hidalgo CG, Granzier HL, Vonk-Noordegraaf A, van der Velden J, de Man FS. Right ventricular diastolic impairment in patients with pulmonary arterial hypertension. *Circulation* 2013;128:2016–2025.

Rudski LG, Lai WW, Afilalo J, Hua L, Handschumacher MD, Chandrasekaran K, Solomon SD, Louie EK, Schiller NB. Guidelines for the echocardiographic assessment of the right heart in adults: a report from the American Society of Echocardiography endorsed by the European Association of Echocardiography, a registered branch of the European Society of Cardiology, and the Canadian Society of Echocardiography. *J Am Soc Echocardiogr* 2010;23:685–713.

Sade LE, Gulmez O, Eroglu S, Sezgin A, Muderrisoglu H. Noninvasive estimation of right ventricular filling pressure by ratio of early tricuspid inflow to annular diastolic velocity in patients with and without recent cardiac surgery. *J Am Soc Echocardiogr* 2007;20:982–988.

Senzaki H, Kass DA. Analysis of isovolumic relaxation in failing hearts by monoexponential time constants overestimates lusitropic change and load dependence: mechanisms and advantages of alternative logistic fit. *Circ Heart Fail* 2010;3:268–276.

Shiina Y, Funabashi N, Lee K, Daimon M, Sekine T, Kawakubo M, Takahashi M, Yajima R, Tanabe N, Kuriyama T, Komuro I. Right atrium contractility and right ventricular diastolic function assessed by pulsed tissue Doppler imaging can predict brain natriuretic peptide in adults with acquired pulmonary hypertension. *Int J Cardiol* 2009;135:53–59.

Shmuylovich L, Kovács SJ. Load-independent index of diastolic filling: model-based derivation with in vivo validation in control and diastolic dysfunction subjects. *J Appl Physiol (1985)* 2006;101:92–101.

Shmuylovich L, Kovács SJ. E-wave deceleration time may not provide an accurate determination of LV chamber stiffness if LV relaxation/viscoelasticity is unknown. *Am J Physiol Heart Circ Physiol* 2007;292:H2712–2720.

Sundereswaran L, Nagueh SF, Vardan S, Middleton KJ, Zoghbi WA, Quiñones MA, Torre-Amione G. Estimation of left and right ventricular filling pressures after heart transplantation by tissue Doppler imaging. *Am J Cardiol* 1998;82:352–357.

Yang W, Marsden AL, Ogawa MT, Sakarovitch C, Hall KK, Rabinovitch M, Feinstein JA. Right ventricular stroke work correlates with outcomes in pediatric pulmonary arterial hypertension. *Pulm Circ* 2018;8:2045894018780534.

Yu CM, Lin H, Ho PC, Yang H. Assessment of left and right ventricular systolic and diastolic synchronicity in normal subjects by tissue Doppler echocardiography and the effects of age and heart rate. *Echocardiography* 2003;20:19–27.

Zoghbi WA, Habib GB, Quinones MA. Doppler assessment of right ventricular filling in a normal population. Comparison with left ventricular filling dynamics. *Circulation* 1990;82:1316–1324.

Figure captions list

Figure 1

Quantitation of diastolic function via the PDF formalism.

Representative transtricuspid E-wave Doppler images from a normal subject (A, B) and a PAH patient (C, D) are shown. Doppler E-wave velocity profile edge detection and fitted curves were shown. The digitized E-wave maximum velocity envelope is identified (A, C) and fitted using the Levenberg-Marquardt method by the solution to the PDF model (B, D), which yielded the 3 unique best fit PDF parameters of chamber stiffness k, relaxation c, and initial load x_0.

Control subject (A, B) parameters: x_0 = 11.4 cm, c = 10.1 g/s, k = 88.6 g/s^2; MSE 5.3 cm^2/s^2.

PAH patient (C, D) parameters: x_0 = 9.2 cm, c = 27.7 g/s, k = 148.1 g/s^2; MSE 5.1 cm^2/s^2.

Figure 2

Conventional and kinematic model-based RV diastolic parameters.

The values of E/A (A), E/e′ (B), DT (C), k (D), c (E), and x_0 (F) were compared between the control and the PAH groups.

Boxes, IQR; Central line, median; Whiskers, minimum and maximum.

Figure 3

Correlation between the kinematic model parameters and RV performance in patients with PAH

RVFAC had no significant correlation with k (A), c (B), and x_0 (C). There was significant correlation between TRPG and k (D), whereas there were no significant correlation with c (E) and x0 (F). Linear regression lines with the 95% confidence interval (dashed

lines) are indicated. RVFAC, right ventricular fractional area change; TRPG, tricuspid regurgitation peak gradient

1 Table 1. Clinical characteristics of the participants
2
3

	Control (n = 34)	PAH (n = 10)	p values
Sex (male/female)	15/19	4/6	n.s.
Age (y)	11.3 ± 3.4 (7 – 19)	12.8 ± 5.4 (8 – 19)	n.s.
Weight (kg)	38.6 ± 13.4 (17.1 - 66.0)	39.2 ± 15.1 (20.2 – 63.1)	n.s.
Height (cm)	141.4 ± 20.6 (18.0 – 172.2)	144.9 ± 18.1 (112.0 – 171.0)	n.s.
Body surface area (m^2)	1.21 ± 0.34 (0.71 – 1.73)	1.24 ± 0.33 (0.77 – 1.67)	n.s.
Heart rate (bpm)	65 ± 11 (52 – 93)	66 ± 11 (54 – 84)	n.s.
Systolic blood pressure (mmHg)	89 ± 14 (72 – 120)	90 ± 14 (77– 115)	n.s.
Diastolic blood pressure (mmHg)	54 ± 10 (37 – 68)	56 ± 9 (38 – 67)	n.s.
LVEDD (mm)	44.8 ± 5.8 (36.0 – 49.8)	40.8 ± 6.8 (31.0 – 49.2)	n.s.
LVFS (%)	44.4 ± 3.9 (38.0 – 48.8)	41.4 ± 4.9 (38 – 48.8)	n.s.
LVEF (%)	70.3 ± 3.4 (64.0 – 78.2)	71.3 ± 6.4 (63.1 – 80.2)	n.s.
RVFAC (%)	50.8 ± 5.9 (43.0 – 60.1)	28.6 ± 5.1 (20.0 – 35.3)	< 0.0001
Transmitral flow	0.95 ± 0.11	0.75±0.19	< 0.0001
E-wave (m/s)	(0.65 – 1.15)	(0.52 – 1.10)	
A-wave (m/s)	0.41 ± 0.12 (0.15 – 0.59)	0.60 ± 0.15 (0.45 – 0.89)	0.0002
Transtricuspid flow	0.51 ± 0.09	0.40± 0.07	0.0010
E-wave (m/s)	(0.34 – 0.73)	(0.29 – 0.52)	
A-wave (m/s)	0.31± 0.10 (0.11 – 0.49)	0.41 ± 0.13 (0.25 – 0.62)	0.0130
Mitral annular motion	18.6 ± 2.4	9.3 ± 2.2	< 0.0001
e′ wave (cm/s)	(13.2 – 24.0)	(5.6 – 12.2)	
a′ wave (cm/s)	6.7 ± 1.8 (4.1 – 11.1)	10.3 ± 2.3 (6.8 – 12.9)	< 0.0001
s′ wave (cm/s)	9.9 ± 1.9 (6.8 – 12.9)	8.4 ± 2.1 (5.6 – 11.1)	0.0378
Tricuspid annular motion	13.5 ± 2.9	8.9 ± 1.7	< 0.0001
e′ wave (cm/s)	(9.5 – 19.0)	(6.7 – 12.5)	
a′ wave (cm/s)	7.6 ± 2.3 (4.6 – 13.0)	12.9 ± 2.8 (9.5 – 18.5)	< 0.0001
s′ wave (cm/s)	12.5 ± 3.92 (8.5 – 16.2)	10.2 ± 2.1 (6.5 – 13.5)	n.s.
TRPG (mmHg)	—	50.4 ± 11.9 (41 – 80)	—
Time on treatment (years)		5.1 ± 3.4 (2 – 12)	
Treatment		Epoprostenol 2 Bosentan 3	

Macitentan	7
Tadarafil	9

Data are shown as mean ± SD, with the range shown in parentheses.
LVEDD, left ventricular end-diastolic dimension; LVEF, left ventricular ejection fraction; LVFS, left ventricular fractional shortening; RVFAC, right ventricular fractional area change; TRPG, tricuspid regurgitation peak gradient; n.s., not significant.

Table 2. Comparison of the kinematic model-based parameters between LV and RV in normal subjects

	Normal LV (n = 34)	Normal RV (n = 34)	p values
k (g/s^2)	247.3 ± 59.4 (140.6 – 385.5)	135.7 ± 49.5 (44.9 – 263.5)	< 0.0001
c (g/s)	17.5 ± 5.8 (7.6 – 29.5)	10.6 ± 5.2 (3.0 – 20.6)	< 0.0001
x_0 (cm)	11.7 ± 2.4 (7.8 – 16.0)	8.2 ± 2.9 (3.9 – 13.8)	< 0.0001
MSE (cm^2/s^2)	29.2 ± 15.9 (5.3 – 69.4)	8.3 ± 5.0 (1.8 – 25.4)	< 0.0001

Data are shown as mean ± SD, with the range shown in parentheses.
MSE, mean square error; n.s., not significant.

Table 3. Comparison of RV diastolic functional parameters between the control and PAH groups

	Normal RV (n = 34)	PAH RV (n =10)	p values
E-peak (m/s)	0.51 ± 0.09 (0.34 – 0.73)	0.40 ± 0.07 (0.29 – 0.52)	0.0010
A-peak (m/s)	0.31 ± 0.10 (0.11 – 0.49)	0.41 ± 0.13 (0.25 – 0.62)	0.0130
AT (ms)	111.9 ± 24.3 (71 – 199)	80.1 ± 8.4 (64 – 91)	< 0.0001
DT (ms)	192.1 ± 63.0 (113 – 395)	201.9 ± 106.5 (110 – 367)	n.s.
E/A	1.83 ± 0.73 (0.89 – 3.70)	1.07 ± 0.33 (0.61 – 1.69)	0.0003
e′ (cm/s)	13.5 ± 2.9 (9.5 – 19.0)	8.9 ± 1.7 (6.7 – 12.5)	< 0.0001
a′ (cm/s)	7.6 ± 2.3 (4.6 – 13.0)	12.9 ± 2.8 (9.5 – 18.5)	< 0.0001
e′/a′	1.9 ± 0.5 (0.91 – 2.9)	0.7 ± 0.2 (0.49 – 1.1)	< 0.0001
E/e′	3.9 ± 1.1 (2.1 – 6.5)	4.7 ± 1.1 (2.8 – 6.6)	n.s.
k (g/s^2)	135.7 ± 49.5 (44.9 – 263.5)	182.5 ± 72.4 (106.5 – 368.8)	0.0232
c (g/s)	10.6 ± 5.2 (3.0 – 20.6)	21.9 ± 6.5 (12.1 – 34.5)	< 0.0001
x_0 (cm)	8.2 ± 2.9 (3.9 – 13.8)	7.7 ± 2.4 (4.0 – 11.2)	n.s.
MSE (cm^2/s^2)	8.3 ± 5.0 (1.8 – 25.4)	5.3 ± 5.3 (0.8 – 17.2)	n.s.
c^2-4k (s^{-2})	-404.2 ± 196.3 (-884.1 – -37.3)	-210.9±504.9 (-1136.8 – 762.5)	n.s.
kx_0 (dyn)	1039.2 ± 361.8 (388.5 – 2156.3)	1270.3 ± 168.9 (951.0 – 1482.2)	0.0238
$1/2kx_0^2$ (erg)	4480.8 ± 1731.2 (1001.9 – 11301.3)	4916.9 ± 1815.8 (2184.2 – 7706.0)	0.0458
cE-peak (dyn)	544.0 ± 300.3 (141.8 – 1344.1)	857.5 ± 1704.1 (471.4 – 1072.1)	0.0026

Data are shown as mean ± SD, with the range shown in parentheses.
AT, E-wave acceleration time; DT, E-wave deceleration time; MSE, mean square error; n.s., not significant.

Table 4. Intra-observer and inter-observer reproducibility

	Intra-observer variation			Inter-observer variation		
	ICC (95% CI)	p	Bland-Altman Bias (95% LOA)	ICC (95% CI)	p	Bland-Altman Bias (95% LOA)
E-peak (m/s)	0.987 (0.967 – 0.995)	<0.0001	-0.005 (-0.04 to 0.03)	0.951 (0.877 – 0.980)	<0.0001	-0.028 (-0.10 to 0.04)
A-peak (m/s)	0.910 (0.787 – 0.964)	<0.0001	0.009 (-0.08 to 0.10)	0.882 (0.720 – 0.953)	<0.0001	-0.001 (-0.11 to 0.10)
AT (ms)	0.803 (0.559 – 0.919)	<0.0001	-0.9 (-21.7 to 20.0)	0.743 (0.448 – 0892)	0.0002	1.1 (-23.1 to 25.2)
DT (ms)	0.954 (0.885 – 0.982)	<0.0001	2.6 (-52.4 to 57.5)	0.946 (0.867 – 0.979)	<0.0001	-19.3 (-88.2 to 49.5)
e′ (cm/s)	0.965 (0.911 – 0.986)	<0.0001	0.230 (-1.25 to 1.71)	0.944 (0.862 – 0.978)	<0.0001	0.400 (-1.44 to 2.24)
a′ (cm/s)	0.990 (0.974 – 0.996)	<0.0001	0.000 (-1.13 to 1.13)	0.981 (0.953 – 0.993)	<0.0001	0.130 (-1.44 to 1.70)
k (g/s^2)	0.893 (0.744 – 0.957)	<0.0001	-0.205 (-42.16 to 38.05)	0.839 (0.630 – 0.935)	<0.0001	0.498 (-48.00 to 48.99)
c (g/s)	0.899 (0.7522 – 0.961)	<0.0001	1.452 (-5.01 to 7.92)	0.896 (0.746 – 0.960)	<0.0001	2.621 (-4.39 to 9.64)
x_0 (cm)	0.891 (0.739 – 0.956)	<0.0001	-0.1 (-1.5 to 1.6)	0.815 (0.582 – 0.924)	<0.0001	-0.3 (-2.5 to 2.7)

Data are shown as mean ± SD, with the range shown in parentheses.
ICC, intraclass correlation coefficient; LOA, limits of agreement defined as the mean difference ± 1.96 SD of differences; n.s., not significant.

Figure 1

Click here to access/download;Figure;Figure 1 .eps

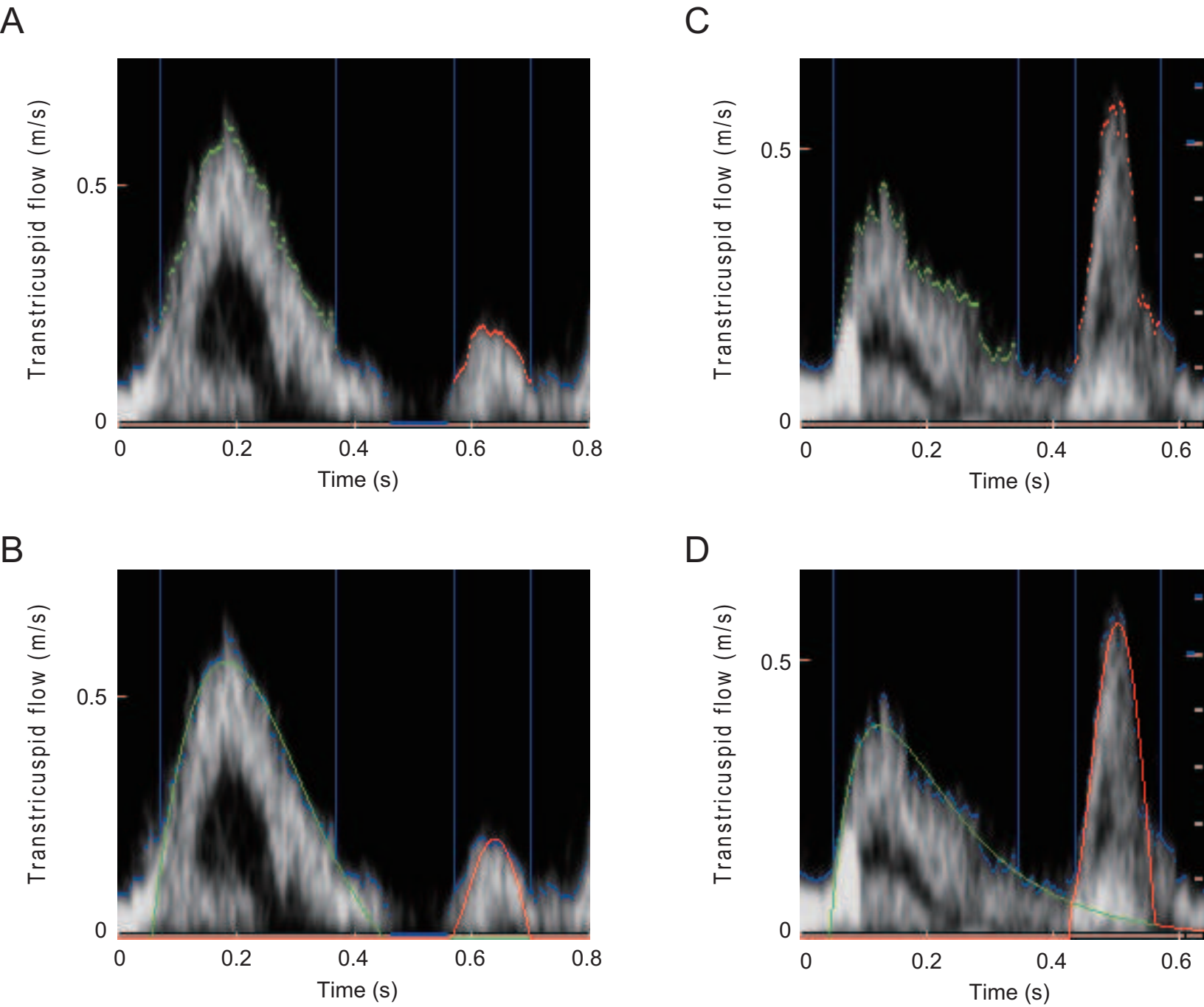

Figure 2

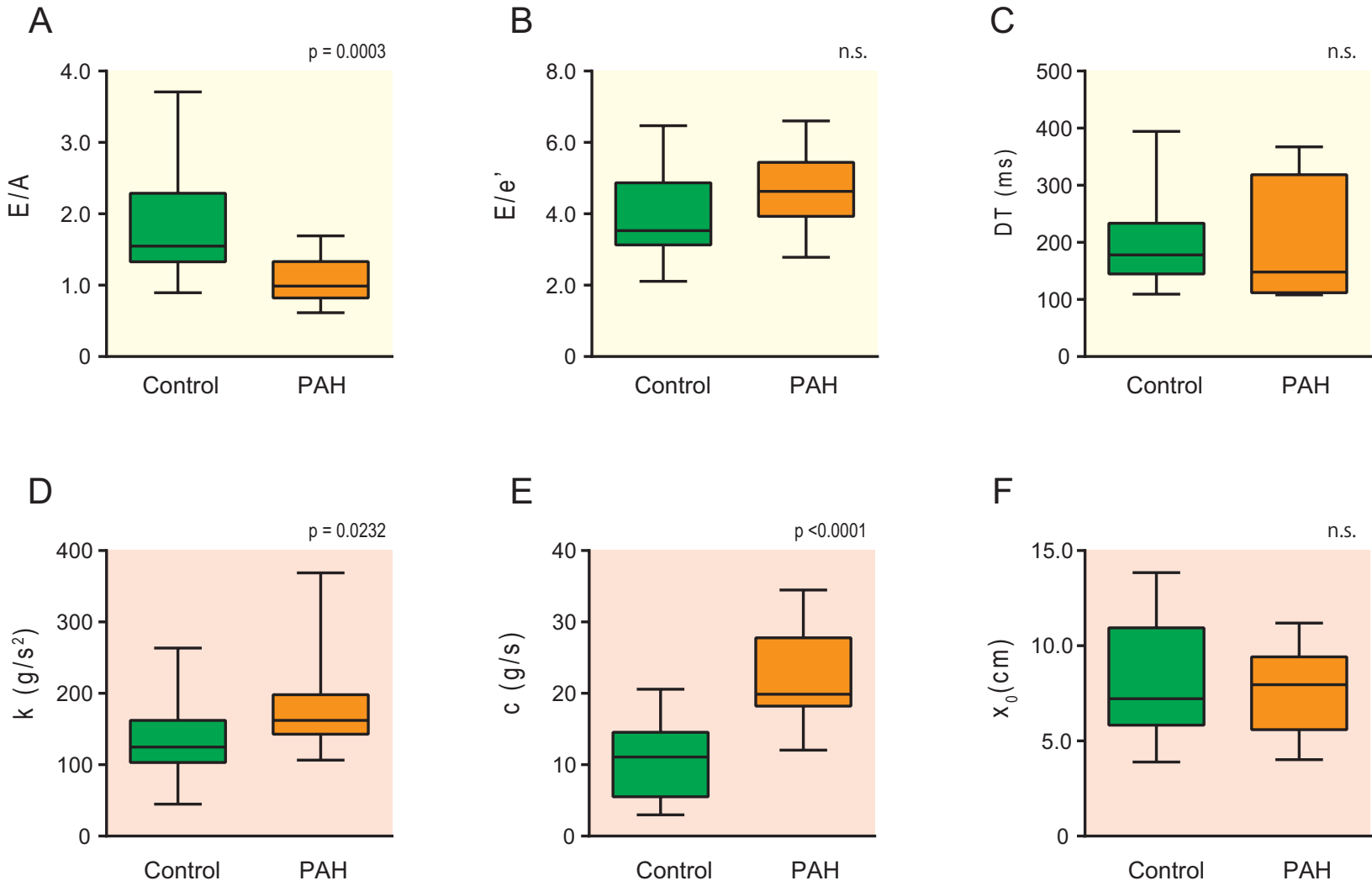

Figure 3

Click here to access/download;Figure;Fig 3.eps